Available online at www.sciencedirect.com
ScienceDirect
Journal of Sound and Vibration 306 (2007) 333–348
JOURNAL OF SOUND AND VIBRATION
www.elsevier.com/locate/jsvi

Vibration analysis of functionally graded thin-walled rotating blades under high temperature supersonic flow using the differential quadrature method

S.A. Fazelzadeh[a,*], P. Malekzadeh[b], P. Zahedinejad[a], M. Hosseini[a]

[a]*Department of Mechanical Engineering, Shiraz University, Shiraz 71344, Islamic Republic of Iran*
[b]*Department of Mechanical Engineering, Persian Gulf University, Bushehr 75168, Islamic Republic of Iran*

Received 26 May 2006; received in revised form 3 May 2007; accepted 3 May 2007
Available online 27 June 2007

Abstract

In this study, differential quadrature (DQ) vibration analysis of a rotating thin walled-blade made of functionally graded materials (FGMs) operating under high temperature supersonic gas flow is investigated. The governing equations are based on the first-order shear deformation theory of beams which include the effects of the rotary inertias and the blade presetting angle. Quasi-steady aerodynamic pressure loadings and steady wall temperature assumptions are made. The explicit DQ-discretized form of the equations of motion and the related boundary conditions are presented. The convergence of the method is examined and to verify its accuracy, the results are compared with those of the Galerkin method where excellent agreements are observed. The effects of the Mach number, rotating speed, geometric parameters and blade material properties on the natural frequencies are examined.

1. Introduction

Advanced rotating turbomachinery blades operate at high speed and temperature gas flow environment. In the future rocket engine applications, such as the Reusable Launch Vehicle (RLV), the Fastrac supersonic ones, their turbine blades are going to be exposed to a supersonic flow field [1,2].

The dynamic response characteristics of rotating blades can be dramatically affected by the high temperatures in which the blades should operate [3–6]. Moreover, as a result of the high speed airflow, static and dynamic instabilities can occur. Therefore, the ability to predict the aerothermoelastic behavior of such structural components becomes of great practical importance.

Functionally graded materials (FGMs), for high temperature structural applications, are microscopically inhomogeneous special composites, whose thermo-mechanical properties vary smoothly and continuously in predetermined directions throughout the body of the structure. This feature is achieved by gradually varying the volume fraction of constituent materials, which are usually made of ceramics and metals.

*Corresponding author.
E-mail address: Fazelzad@shirazu.ac.ir (S.A. Fazelzadeh).

0022-460X/$ - see front matter © 2007 Elsevier Ltd. All rights reserved.
doi:10.1016/j.jsv.2007.05.011

Nomenclature

a blade width
a_{ij} stiffness quantities
A_{ij} first-order weighting coefficients
b blade height
b_k mass quantities
B_{ij} second-order weighting coefficients
C_∞ sound speed
E Young's modulus
$\mathbf{G}$ aerodynamic damping matrix
h wall thickness
$\mathbf{i}$ unit vector along the x-axis
$\mathbf{j}$ unit vector along the y-axis
$\mathbf{k}$ unit vector along the z-axis
k volume fraction parameter
K thermal conductivity
L blade length
$\mathbf{M}$ mass matrix
M_∞ Mach number
M_x, M_y moments about the x and y axes
p_x, p_y distributed force in x- and y-direction
Q_x, Q_y shear forces in the x- and y-directions
$\mathbf{R}$ position vector of an arbitrary point of the blade
R_f steady temperature recovery factor
R_0 Hub radius
s, n local surface coordinates (tangential, normal to mid-surface)
$\mathbf{S}$ stiffness matrix
$\mathbf{S_{bd}}$, $\mathbf{S_{db}}$, $\mathbf{S_{dd}}$ boundary–domain interaction stiffness matrix, domain–boundary interaction stiffness matrix, domain stiffness matrix, respectively
T_∞ air flow temperature
T_z axial force in the z direction
u, v, w displacement components in x, y, z coordinate
u_0, v_0 displacement components in x and y direction
U_0, V_0 amplitude of displacement components in x and y direction
$\mathbf{U_b}$, $\mathbf{U_d}$ boundary and domain degrees of freedom vectors, respectively
$U^t_{x^p}$, $U^t_{y^p}$ tangential components of fluid velocity on the positive x^p and y^p planes
U_∞ air flow velocity
x, y, z blade coordinate
x^P, y^P, z^P principle coordinate
α thermal expansion coefficient
β, β_0 pretwist angle of an arbitrary cross section and tip cross section, respectively
γ setting angle
δT, δV, δW_e variation of kinetic and potential energy and virtual work of external force, respectively
Δp_{x^p}, Δp_{y^p} x and y aerodynamic loading on the positive x^p and y^p planes
ΔT steady-state temperature raise
ε_{ij} strain tensor components
θ_x, θ_y rotation about x and y axes, respectively
Θ_x, Θ_y amplitude of rotation about x and y axis, respectively
κ air polytropic ratio
κ_s transverse shear correction factor
ν Poisson's ratio
ξ $C_\infty \rho_\infty$
ρ material mass density
ρ_∞ air flow density
σ_{ij} stress tensor components
ω_i natural frequency
$\bar{\omega}_i$ non-dimensional imaginary part of natural frequency ($\omega_{Ii} L^2 \sqrt{b_1/a_{33}}$)
Ω rotating speed
$\bar{\Omega}$ non-dimensional angular velocity of the shaft $\Omega(L^2\sqrt{b_1/a_{33}})$
$(\dot{.}), (.)'$ $\mathrm{d}/\mathrm{d}t(.)$, $\mathrm{d}/\mathrm{d}z(.)$
$(\,)^i, (\,)^i_{,z}$ $(\,)|_{z=z_i}$, $\mathrm{d}(\,)/\mathrm{d}z|_{z=z_i}$

In addition to the research work developed based on the theory of elasticity for the analysis of FGM beams and plates [7–10], the classical beam theory has also been used to study the behavior of thin-walled structures made of FGMs [3–5,11].

The research work related to the modeling and behavior of rotating blades made of FGMs and operating at high temperature environment, to the best of the authors' knowledge, have been limited to those of Librescu and his co-workers [3–5]. In the previous studies of rotating FGMs thin-walled blades at high temperature environment, aerothermoelastic loading has not been considered. More recently, Fazelzadeh and Hosseini [11] have investigated aerothermoelastic behavior of the rotating FGMs thin-walled blade under supersonic flow.

In all these works, the Galerkin method was used to solve the governing equations. In addition to the intrinsic complexities involving the modeling of these structures, another intervening issue is the solution of their variable-coefficient governing equations in a simple and computationally efficient manner.

Differential quadrature method (DQM), as an efficient alternative numerical tool for structural analysis, was prompted by Bert et al. [12] in 1988. Applying the method to such problems, it was concluded that DQM procedures offer comparable accuracy with less computational effort in comparison with those of Rayleigh–Ritz method, Galerkin method, finite difference and finite element method (FEM) [12,13]. The method has been widely used for static and free vibration analysis of beams and plates [14–18]. A review of the early developments in DQM can be found in Bert and Malik [13].

In the present work, the applicability of DQM as an efficient numerical method for vibration analysis of rotating thin walled-beam blade made of FGMs under the aerothermoelastic loading is demonstrated. The governing equations are based on the first-order shear deformation beam theory which includes the effects of the presetting angle and the rotary inertia. The effects of steady wall temperature and quasi-steady aerodynamic pressure loadings due to flow motion are also included. Due to aerothermoelastic terms in loading, the damping effects are generated in the equations of motion. The DQ discretized form of the governing equations and the related boundary conditions at the domain and boundary grid points are obtained. The accuracy and convergence behavior of the method of solution is demonstrated and the results are compared with those of the Galerkin method [11].

2. Blade geometrical descriptions

Consider a straight and pretwisted flexible blade of length L mounted on a rigid hub of radius R_0, which rotates at constant speed Ω about an axis normal to the longitudinal axis of the blade, as shown in Fig. 1. The blade is allowed to vibrate flexurally in a plane making an angle γ, referred to as the setting angle, with the plane of rotation. In Fig. 1, the coordinate variables of centroidal rotating coordinate system are denoted by x, y and z with its origin located at the blade root. Moreover, the principal coordinate system along the principle axes of an arbitrary blade cross section is chosen with its coordinate variables defined as x^p, y^p and z^p. The two coordinate system are related via the following transformation

$$\begin{aligned} x(s,z) &= x^p(s)\cos(\beta(z)+\gamma) - y^p(s)\sin(\beta(z)+\gamma),\\ y(s,z) &= x^p(s)\sin(\beta(z)+\gamma) + y^p(s)\cos(\beta(z)+\gamma), \quad z(s) = z^p, \end{aligned} \tag{1}$$

where $\beta(z) = \beta_0 z/L$ denotes the pretwist angle of a current beam cross section. It is also appropriate to define the beam surface coordinates system (s, z, n) where s and n are the circumferential and thickness coordinate variables, respectively (see Fig. 1).

3. The basic formulations

Assuming an isotropic material, the corresponding thermoelastic constitutive law, adopted to the case of thin-walled structures, is expressed as

$$\begin{bmatrix} \sigma_{ss} \\ \sigma_{zz} \\ \sigma_{zn} \\ \sigma_{ns} \\ \sigma_{sz} \end{bmatrix} = \begin{bmatrix} Q_{11} & Q_{12} & 0 & 0 & 0 \\ Q_{12} & Q_{22} & 0 & 0 & 0 \\ 0 & 0 & Q_{44} & 0 & 0 \\ 0 & 0 & 0 & Q_{44} & 0 \\ 0 & 0 & 0 & 0 & Q_{66} \end{bmatrix} \begin{bmatrix} \varepsilon_{ss} \\ \varepsilon_{zz} \\ \varepsilon_{zn} \\ \varepsilon_{ns} \\ \varepsilon_{sz} \end{bmatrix} - \begin{bmatrix} \hat{\alpha}\Delta T \\ \hat{\alpha}\Delta T \\ 0 \\ 0 \\ 0 \end{bmatrix}, \tag{2}$$

where

$$Q_{11} = \frac{E}{1-\nu^2}, \quad Q_{12} = \frac{E\nu}{1-\nu^2}, \quad Q_{66} = \frac{E}{2(1+\nu)}, \quad Q_{44} = Q_{55} = k_s^2\frac{E}{2(1+\nu)}, \quad \hat{\alpha} = \frac{E}{1-\nu}\alpha.$$

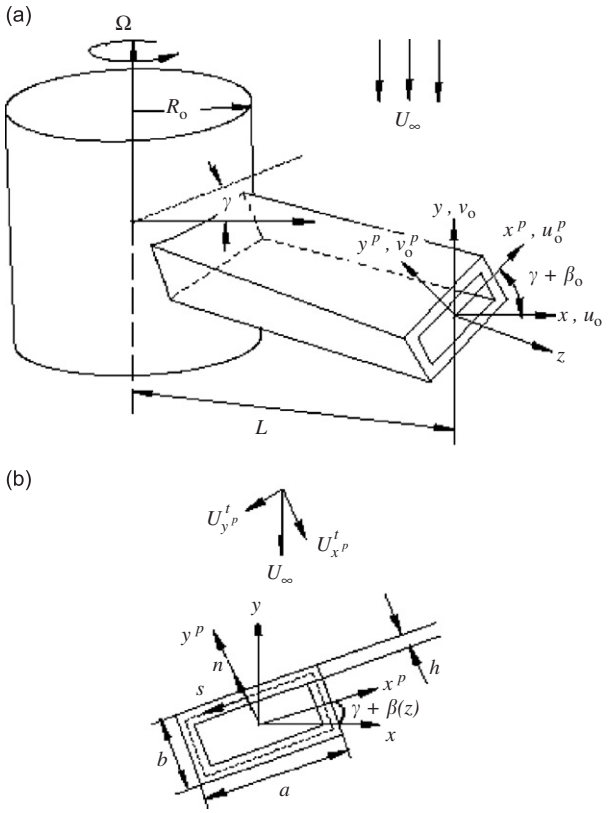

Fig. 1. Geometry of the rotating blades: (a) pretwisted thin-walled blade, and (b) blade cross section.

For a model of ceramic/metal FGM, the material properties vary continuously across the blade thickness according to [19]

$$PM(n) = (PM_c - PM_m)\ V_m + PM_m, \quad V_c = 1 - V_m. \tag{3}$$

Herein the subscripts m and c identify quantities associated with the metal and ceramic, respectively. PM in Eq. (3) is material properties corresponding to modulus of elasticity, Poisson's ratio, density, thermal expansion coefficient and thermal conductivity. For the case of a uniform blade thickness, V_m can be expressed as

$$V_m = \left[\frac{2n+h}{2h}\right]^k, \tag{4}$$

where k ($0 \leqslant k \leqslant \infty$) is the volume fraction parameter. This shows that the material properties vary continuously from fully ceramic at the top surface of the blade to fully metal at the bottom surface.

Based on the experimental observations [5], it is known that the properties of FGM are temperature-dependent and this can be generally expressed as

$$P(n) = P_0(P_{-1}/T + 1 + P_1 T + P_2 T^2 + P_3 T^3), \tag{5}$$

where P_0, P_{-1}, P_1, P_2, P_3 are thermal property constants and T (in K) is the environmental temperature. For constitutes considered in this paper, namely silicon nitride (SN) and stainless steel (SS), the constants P_i are supplied in Refs. [5,20].

A steady-state one-dimensional temperature distribution through the thickness is assumed for the blade, which is governed by the following differential equation and boundary conditions

$$\frac{\mathrm{d}}{\mathrm{d}n}\left[K(n)\frac{\mathrm{d}T}{\mathrm{d}n}\right] = 0, \quad T\left(n = -\frac{h}{2}\right) = T_m, \quad T\left(n = \frac{h}{2}\right) = T_c. \tag{6}$$

It is assumed that the blade is exposed to supersonic gas flow. Therefore, the temperature difference can be expressed as [21],

$$\Delta T = T_c - T_\infty = R_f[(\kappa - 1)/2]M_\infty^2 T_\infty, \tag{7}$$

where T_c is the blade wall temperature.

The first-order piston theory is used to evaluate the perturbed gas pressure. Hence, the pressure on the principal planes of the blade become

$$\Delta P_{y^p} = C_\infty \rho_\infty \left(\frac{\partial v^p}{\partial t} + U^t_{y^p}\frac{\partial v^p}{\partial z}\right), \quad \Delta P_{x^p} = C_\infty \rho_\infty \left(\frac{\partial u^p}{\partial t} + U^t_{x^p}\frac{\partial u^p}{\partial z}\right), \tag{8}$$

where

$$U^t_{x^p} = U_\infty \cos(\beta + \gamma), \quad U^t_{y^p} = U_\infty \sin(\beta + \gamma). \tag{9}$$

Herein, C_∞, ρ_∞, U_∞ are the speed of sound, the free stream air density and velocity; $U^t_{x^p}$ and $U^t_{y^p}$ are the tangential components of the fluid velocity on the positive x^p and y^p planes, respectively. Also, u^p and v^p are displacement components along the principal axes x^p and y^p, which are related to the displacement components in x–y coordinate system as

$$u^p = u_0 \cos(\beta + \gamma) + v_0 \sin(\beta + \gamma), \quad v^p = -u_0 \sin(\beta + \gamma) + v_0 \cos(\beta + \gamma). \tag{10}$$

Using Eq. (8), the external loads per unit axial length distributed in the x- and y-directions can be obtained, respectively, as

$$p_x = a\Delta P_{y^p}\sin(\beta + \gamma) - b\Delta P_{x^p}\cos(\beta + \gamma), \quad p_y = -a\Delta P_{y^p}\cos(\beta + \gamma) - b\Delta P_{x^p}\sin(\beta + \gamma). \tag{11}$$

The governing equations and boundary conditions can be derived via the extended Hamiltonian's principle,

$$\int_{t_1}^{t_2} (\delta T - \delta V + \delta W_e)\mathrm{d}t = 0. \tag{12}$$

In the above equation, the variation of kinetic energy is given by

$$\delta T = \int_o^L (\rho \dot{\mathbf{R}}.\delta\dot{\mathbf{R}})\mathrm{d}z \tag{13}$$

in which,

$$\dot{\mathbf{R}} = [\dot{u} + (R_0 + z + w)\Omega]\mathbf{i} + \dot{v}\mathbf{j} + [\dot{w} - (x + u)\Omega]\mathbf{k}.$$

Also, the variation of strain energy based on the first-order shear deformation theory of beams can be written as

$$\begin{aligned}\delta V = & -\int_0^L \{(M_y' - Q_x)\delta\theta_y + (M_x' - Q_y)\delta\theta_x + [Q_x' + (T_z u_0')']\delta u_0 + [Q_y' + (T_z v_0')']\delta v_0\}\mathrm{d}z \\ & + [M_y\delta\theta_y + M_x\delta\theta_x + (Q_x + T_z u_0')\delta u_0 + (Q_y + T_z v_0')\delta v_0]\big|_0^L,\end{aligned} \tag{14}$$

δW_e is the virtual work of non-conservative external forces, which in this study becomes

$$\delta W_e = \int_0^L (p_x\delta u_0 + p_y\delta v_0)\mathrm{d}z. \tag{15}$$

Substituting Eqs. (13)–(15) into Eq. (12) and using the integration by part method, the equations of motion and the related boundary conditions can be obtained as

Governing equations:

$$\delta u_0 : [a_{44}(z)(u_0' + \theta_y) + a_{45}(z)(v_0' + \theta_x)]' - b_1\ddot{u}_0 + b_1 u_0\Omega^2 + \Omega^2[R(z)u_0']' + p_x = 0, \tag{16}$$

$$\delta v_0 : [a_{55}(z)(v_0' + \theta_x) + a_{45}(z)(u_0' + \theta_y)]' - b_1\ddot{v}_0 + \Omega^2[R(z)v_0']' + p_y = 0, \tag{17}$$

$$\delta\theta_y : [a_{22}(z)\theta'_y + a_{23}(z)\theta'_x]' - a_{44}(z)(u'_0 + \theta_y) - a_{45}(z)(v'_0 + \theta_x) - (b_5(z) + b_{15}(z))(\ddot{\theta}_y - \Omega^2\theta_y) - (b_6(z) - b_{13}(z))(\ddot{\theta}_x - \Omega^2\theta_x) = 0 \tag{18}$$

$$\delta\theta_x : [a_{33}(z)\theta'_x + a_{32}(z)\theta'_y]' - a_{55}(z)(v'_0 + \theta_x) - a_{54}(z)(u'_0 + \theta_y) - (b_4(z) + b_{14}(z))(\ddot{\theta}_x - \Omega^2\theta_x) - (b_6(z) - b_{13}(z))(\ddot{\theta}_y - \Omega^2\theta_y) = 0, \tag{19}$$

where the stiffness quantities $a_{ij} = a_{ji}$ are given in Ref. [5].

Boundary conditions:

$$\text{At} \quad z = 0 : \quad u_0 = v_0 = \theta_y = \theta_x = 0. \tag{20}$$

$$\text{At} \quad z = L : \quad \delta u_0 : a_{44}(u'_0 + \theta_y) + a_{45}(v'_0 + \theta_x) = 0, \tag{21}$$

$$\delta v_0 : a_{55}(v'_0 + \theta_x) + a_{54}(u'_0 + \theta_y) = 0, \tag{22}$$

$$\delta\theta_y : a_{22}\theta'_y + a_{23}\theta'_x = 0, \tag{23}$$

$$\delta\theta_x : a_{33}\theta'_x + a_{32}\theta'_y = 0. \tag{24}$$

The solution of the above equations of motion may be assumed as follows:

$$u_0(z,t) = U_0(z)e^{\omega t}, \quad v_0(z,t) = V_0(z)e^{\omega t}, \quad \theta_x(z,t) = \Theta_x(z)e^{\omega t}, \quad \theta_y(z,t) = \Theta_y(z)e^{\omega t}. \tag{25}$$

4. DQ discretized form of the governing equations

To establish the eigenvalue problem formulations, the spatial derivatives of the equations of motion and the related boundary conditions are discretized by using DQ discretization rules. A review of differential quadrature method (DQM) is given in Appendix A.

Using the DQ discretization rules for the spatial derivatives and Eq. (25), the DQ analogs of the governing differential equations become,

Eq. (16):

$$\begin{aligned}
&a^i_{44,z}\left(\sum_{j=1}^N A_{ij}U^j_0 + \Theta^i_y\right) + a^i_{44}\left(\sum_{j=1}^N B_{ij}U^j_0 + \sum_{j=1}^N A_{ij}\Theta^j_y\right) + a^i_{45,z}\left(\sum_{j=1}^N A_{ij}V^j_0 + \Theta^i_x\right)\\
&+ a^i_{45}\left(\sum_{j=1}^N B_{ij}V^j_0 + \sum_{j=1}^N A_{ij}\Theta^j_x\right) - b_1\omega^2U^i_0 + b_1\Omega^2U^i_0 + \Omega^2R^i_{,z}\left(\sum_{j=1}^N A_{ij}U^j_0\right) + \Omega^2R^i\left(\sum_{j=1}^N B_{ij}U^j_0\right)\\
&+ a\xi U_\infty(S^i_{\beta\gamma})^2\left(-S^i_{\beta\gamma}\sum_{j=1}^N A_{ij}U^j_0 + C^i_{\beta\gamma}\sum_{j=1}^N A_{ij}V^j_0 - \frac{U^i_0}{L}\beta_0C^i_{\beta\gamma} - \frac{V^i_0}{L}\beta_0S^i_{\beta\gamma}\right)\\
&- b\xi U_\infty(C^i_{\beta\gamma})^2\left(C^i_{\beta\gamma}\sum_{j=1}^N A_{ij}U^j_0 + S^i_{\beta\gamma}\sum_{j=1}^N A_{ij}V^j_0 - \frac{U^j_0}{L}\beta_0S^i_{\beta\gamma} + \frac{V^i_0}{L}\beta_0C^i_{\beta\gamma}\right)\\
&+ a\omega\xi S^i_{\beta\gamma}(-U^i_0S^i_{\beta\gamma} + V^i_0C^i_{\beta\gamma}) - b\omega\xi C^i_{\beta\gamma}(U^i_0C^i_{\beta\gamma} + V^i_0S^i_{\beta\gamma}) = 0,
\end{aligned} \tag{26}$$

Eq. (17):

$$\begin{aligned}
&a^i_{55,z}\left(\sum_{j=1}^N A_{ij}V^j_0 + \Theta^i_x\right) + a^i_{55}\left(\sum_{j=1}^N B_{ij}V^j_0 + \sum_{j=1}^N A_{ij}\Theta^j_x\right) + a^i_{45,z}\left(\sum_{j=1}^N A_{ij}U^j_0 + \Theta^i_y\right)\\
&+ a^i_{45}\left(\sum_{j=1}^N B_{ij}U^j_0 + \sum_{j=1}^N A_{ij}\Theta^j_y\right) - b_1\omega^2V^i_0 + \Omega^2R^i_{,z}\left(\sum_{j=1}^N A_{ij}V^j_0\right) + \Omega^2R^i\left(\sum_{j=1}^N B_{ij}V^j_0\right)
\end{aligned}$$

$$
\begin{aligned}
&- a\xi U_\infty C^i_{\beta\gamma} S^i_{\beta\gamma}\left(-S^i_{\beta\gamma}\sum_{j=1}^{N} A_{ij}U^j_0 + C^i_{\beta\gamma}\sum_{j=1}^{N} A_{ij}V^j_0 - \frac{U^i_0}{L}\beta_0 C^i_{\beta\gamma} - \frac{V^i_0}{L}\beta_0 S^i_{\beta\gamma}\right)\\
&- b\xi U_\infty C^i_{\beta\gamma} S^i_{\beta\gamma}\left(C^i_{\beta\gamma}\sum_{j=1}^{N} A_{ij}U^j_0 + S^i_{\beta\gamma}\sum_{j=1}^{N} A_{ij}V^j_0 - \frac{U^i_0}{L}\beta_0 S^i_{\beta\gamma} + \frac{V^i_0}{L}\beta_0 C^i_{\beta\gamma}\right)\\
&- a\omega C^i_{\beta\gamma}\xi(-U^i_0 S^i_{\beta\gamma} + V^i_0 C^i_{\beta\gamma}) - b\omega S^i_{\beta\gamma}\xi(U^i_0 C^i_{\beta\gamma} + V^i_0 S^i_{\beta\gamma}) = 0,
\end{aligned}
\tag{27}
$$

Eq. (18):

$$
\begin{aligned}
&a^i_{22,z}\left(\sum_{j=1}^{N} A_{ij}\Theta^j_y\right) + a^i_{22}\left(\sum_{j=1}^{N} B_{ij}\Theta^j_y\right) + a^i_{23,z}\left(\sum_{j=1}^{N} A_{ij}\Theta^j_x\right) + a^i_{23}\left(\sum_{j=1}^{N} B_{ij}\Theta^j_x\right) - a^i_{44}\left(\sum_{j=1}^{N} A_{ij}U^j_0 + \Theta^i_y\right)\\
&- a^i_{45}\left(\sum_{j=1}^{N} A_{ij}V^j_0 + \Theta^i_x\right) + (b^i_5 + b^i_{15})\Theta^i_y\Omega^2 + (b^i_6 - b^i_{13})\Theta^i_x\Omega^2 - \omega^2(b^i_5 + b^i_{15})\Theta^i_y\\
&- \omega^2(b^i_6 - b^i_{13})\Theta^i_x = 0,
\end{aligned}
\tag{28}
$$

Eq. (19):

$$
\begin{aligned}
&a^i_{33,z}\left(\sum_{j=1}^{N} A_{ij}\Theta^j_x\right) + a^i_{33}\left(\sum_{j=1}^{N} B_{ij}\Theta^j_x\right) + a^i_{32,z}\left(\sum_{j=1}^{N} A_{ij}\Theta^j_y\right) + a^i_{32}\left(\sum_{j=1}^{N} B_{ij}\Theta^j_y\right) - a^i_{55}\left(\sum_{j=1}^{N} A_{ij}V^j_0 + \Theta^i_x\right)\\
&- a^i_{54}\left(\sum_{j=1}^{N} A_{ij}U^j_0 + \Theta^i_y\right) + (b^i_4 + b^i_{14})\Theta^i_x\Omega^2 + (b^i_6 - b^i_{13})\Theta^i_y\Omega^2 - \omega^2(b^i_4 + b^i_{14})\Theta^i_x\\
&- \omega^2(b^i_6 - b^i_{13})\Theta^i_y = 0.
\end{aligned}
\tag{29}
$$

In a similar manner to those of the equations of motion, the DQ analogs of the boundary conditions can be obtained as

Eq. (20):

$$
U^i_0 = V^i_0 = \Theta^i_y = \Theta^i_x = 0 \quad \text{for} \quad i = 1, \tag{30}
$$

Table 1
Convergence of the first three natural frequencies at various pretwist angles for full ceramic material ($\gamma = 0$, $k = 0$, $M_\infty = 4$)

Pretwist angle β_0 (deg.)	Natural frequencies ($\bar{\omega}_i$)	Number of grid points (N)			
		7	11	13	19
0	1	5.7654	5.7587	5.7588	5.7588
	2	8.5756	8.5731	8.5731	8.5731
	3	21.8834	21.9968	21.9971	21.9969
15	1	5.7675	5.7575	5.7578	5.7575
	2	8.5541	8.5513	8.5515	8.5515
	3	21.9678	22.0616	22.0618	22.0617
30	1	5.7726	5.7539	5.7547	5.7539
	2	8.4894	8.4883	8.4886	8.4883
	3	22.2215	22.2531	22.2531	22.2532
45	1	5.7778	5.7482	5.7490	5.7488
	2	8.3838	8.3896	8.3891	8.3895
	3	22.6441	22.5625	22.5625	22.5626
60	1	5.7804	5.7407	5.7410	5.7408
	2	8.2440	8.2631	8.2630	8.2631
	3	23.2325	22.9768	23.0100	23.0100

Eq. (21):

$$a_{44}^{i}\left(\sum_{j=1}^{N}A_{ij}U_0^j+\Theta_y^i\right)+a_{45}^{i}\left(\sum_{j=1}^{N}A_{ij}V_0^j+\Theta_x^i\right)=0 \quad \text{for} \quad i=N, \tag{31}$$

Eq. (22):

$$a_{55}^{i}\left(\sum_{j=1}^{N}A_{ij}V_0^j+\Theta_x^i\right)+a_{45}^{i}\left(\sum_{j=1}^{N}A_{ij}U_0^j+\Theta_y^i\right)=0 \quad \text{for} \quad i=N, \tag{32}$$

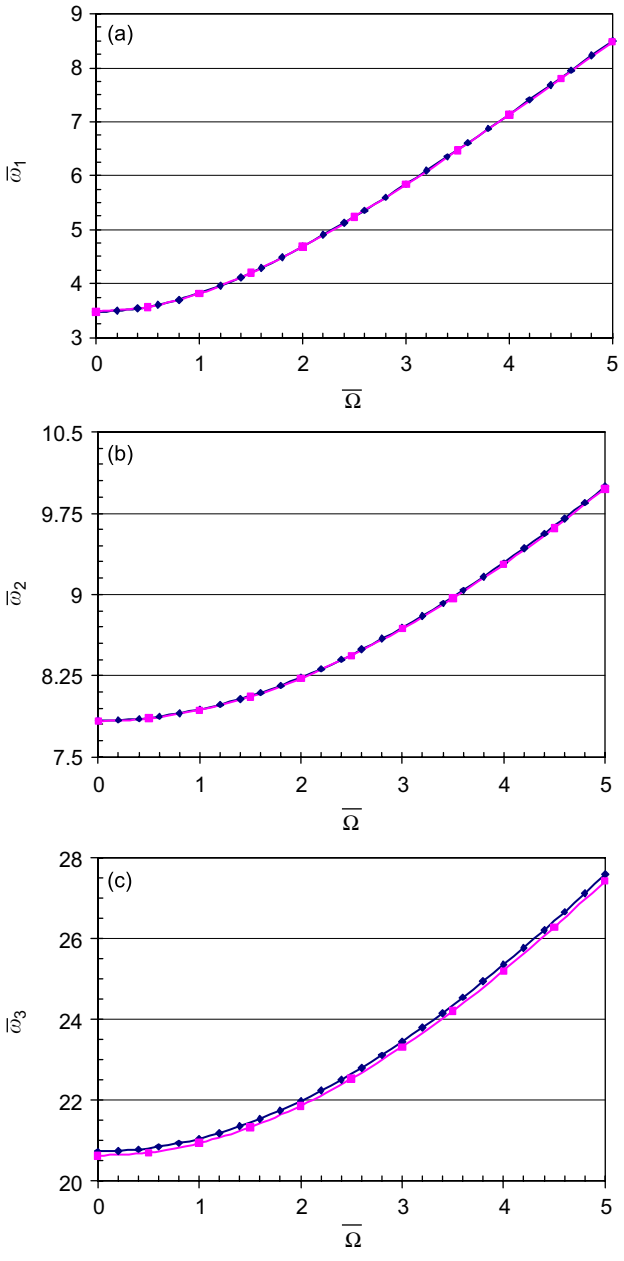

Fig. 2. (a)–(c) Variation of natural frequencies vs. rotating speed (β_0 45°, $\gamma=0$, $k=0$): —◆— Liberscu et al. [5]; —■— present.

Eq. (23):

$$a_{22}^{i}\left(\sum_{j=1}^{N} A_{ij}\Theta_{y}^{j}\right)+a_{23}^{i}\left(\sum_{j=1}^{N} A_{ij}\Theta_{x}^{j}\right)=0 \quad \text{for} \quad i=N, \tag{33}$$

Eq. (24):

$$a_{33}^{i}\left(\sum_{j=1}^{N} A_{ij}\Theta_{x}^{j}\right)+a_{23}^{i}\left(\sum_{j=1}^{N} A_{ij}\Theta_{y}^{j}\right)=0 \quad \text{for} \quad i=N. \tag{34}$$

At the next stage, to setup the eigenvalue system of equations, the degrees of freedom (dof) are separated into domain and boundary dof as

$$\mathbf{U_d}=[\,U_0 \quad V_0 \quad \Theta_y \quad \Theta_x\,]_d^{\mathrm{T}}, \quad \mathbf{U_b}=[\,U_0 \quad V_0 \quad \Theta_y \quad \Theta_x\,]_b^{\mathrm{T}} \tag{35}$$

where the subscripts d and b refer to the domain and the boundary, respectively. Rearranging the discretized equations of motion, the assembled matrix form of the governing equation becomes

$$\mathbf{S_{db}U_b}+\mathbf{S_{dd}U_d}+\omega^2\mathbf{MU_d}+\omega\mathbf{GU_d}=\mathbf{0}. \tag{36}$$

Also, the DQ discretized form of the boundary conditions in matrix form becomes

$$\mathbf{S_{bb}U_b}+\mathbf{S_{bd}U_d}=\mathbf{0}. \tag{37}$$

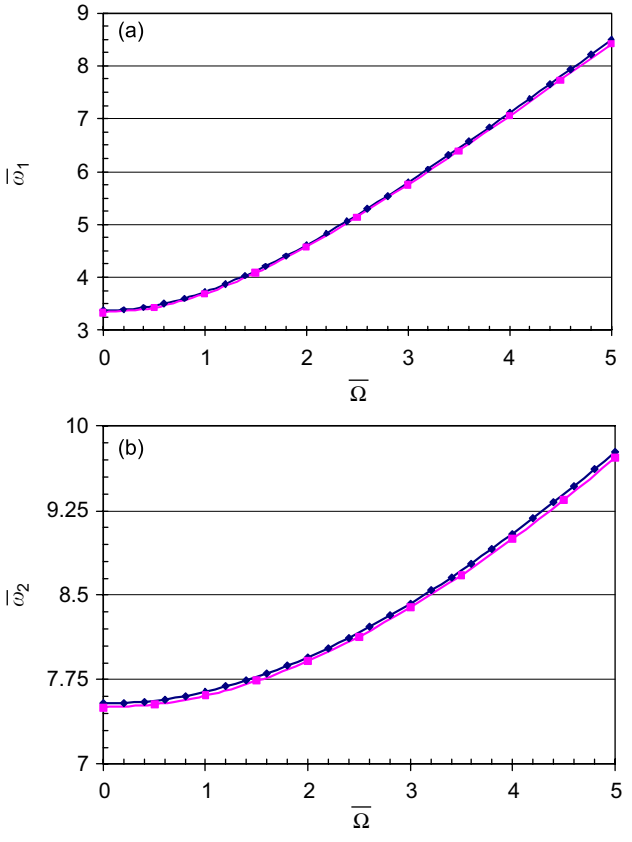

Fig. 3. (a,b) Variation of natural frequencies vs. rotating speed ($M_\infty=4$, β_0 45°, $\gamma=0$, $k=0$): —◆— Galerkin [11]; —■— Present.

In Eqs. (36) and (37), the elements of the coefficient matrixes are obtained based on the definitions of domain and boundary dof vectors. Using Eq. (37) to eliminate $\mathbf{U_b}$ from Eq. (36), one has

$$\mathbf{SU_d} + \omega^2\mathbf{MU_d} + \omega\mathbf{GU_d} = \mathbf{0}, \tag{38}$$

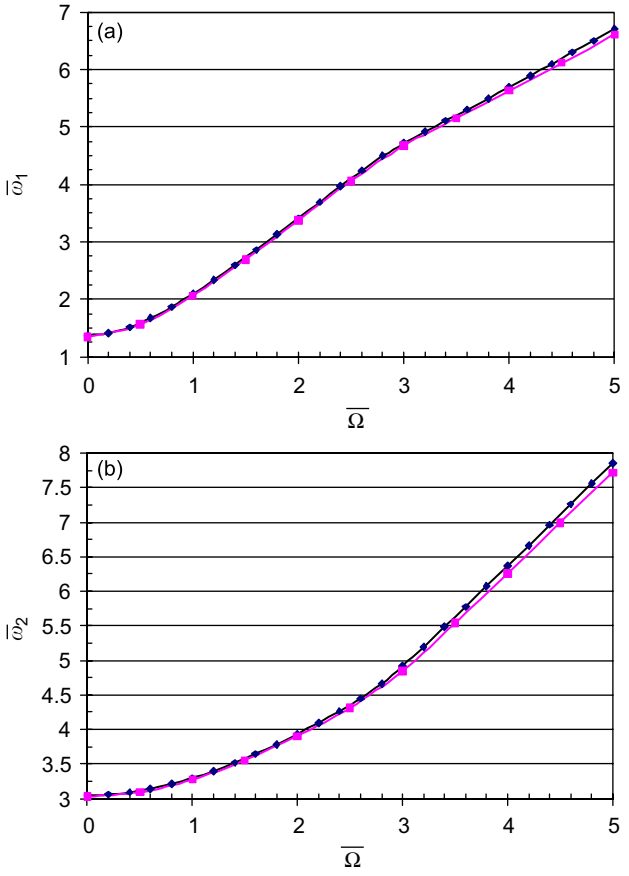

Fig. 4. (a,b). Variation of natural frequencies vs. rotating speed (($M_\infty = 4$, β_0 45°, $\gamma = 0$, $k = 50$): Galerkin [11]; Present.

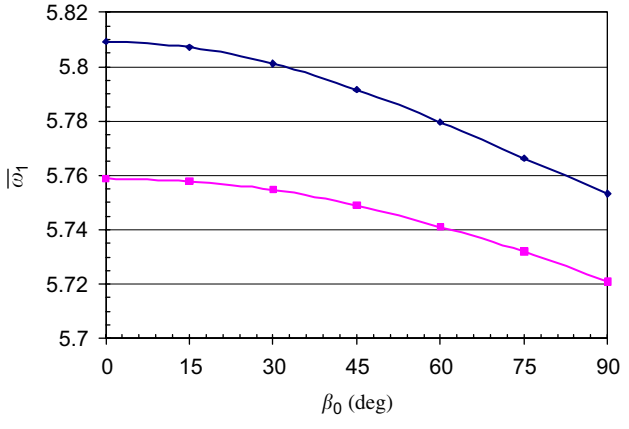

Fig. 5. Variation of natural frequencies vs. pretwist angle ($M_\infty = 4$, $\bar{\Omega} = 3$, $\gamma = 0$, $k = 0$): Galerkin [11]; present.

where

$$\mathbf{S} = \mathbf{S_{dd}} - \mathbf{S_{db}}\mathbf{S_{bb}^{-1}}\mathbf{S_{bd}} = \mathbf{0}.$$

The above equation can be solved to find the natural frequencies as well as the mode shapes. To transform this eigenvalue problem into a standard eigenvalue problem, a new set of dof is defined as

$$\mathbf{X} = \begin{Bmatrix} \mathbf{U} \\ \omega\mathbf{U} \end{Bmatrix}. \tag{39}$$

Using Eq. (39), Eq. (38) can be written as

$$\tilde{\mathbf{A}}\,\mathbf{X} = \omega\mathbf{X}. \tag{40}$$

where the matrix $\tilde{\mathbf{A}}$ is

$$\tilde{\mathbf{A}} = \begin{bmatrix} \mathbf{0} & \mathbf{I} \\ -\mathbf{M^{-1}S} & \mathbf{M^{-1}G} \end{bmatrix}. \tag{41}$$

Herein the matrixes $\mathbf{I}$ and $\mathbf{0}$ are the identity and the null matrix, of order $(4N-8)\times(4N-8)$, respectively. Solving Eq. (41), one obtains the eigenvalues as well as the eigenvectors.

5. Numerical results

At this stage, the convergence and accuracy of the method is verified and the effects of different parameters on the natural frequencies are studied. The thin-walled blade has a uniform rectangular cross section with the following geometric characteristics [5]:

$$R_0 = 1.3\,\text{m}, \quad L = 1.52\,\text{m}, \quad a = 0.257\,\text{m}, \quad b = 0.0827\,\text{m}, \quad h = 0.01654\,\text{m}.$$

Also, the following assumptions are made:

$$\kappa = 1.4, \quad T_\infty = 300\,\text{K}, \quad C_\infty = 340.5\,\text{m/s}, \quad \rho_\infty = 1.1614\,\text{kg/m}^3.$$

In general, the system is non-conservative therefore the stiffness matrix $[S]$ is non-symmetric. The numerical solution leads to $\omega = \omega_R + \mathrm{i}\omega_I$, in which ω_R is a very small value in comparison with ω_I and therefore $\mathrm{e}^{\omega t} \cong \mathrm{e}^{\mathrm{i}\omega_I t}$. At such a critical state, the imaginary part (ω) corresponds to the natural frequency or the flutter frequency of the system.

Firstly, the convergence behavior of the method is investigated by obtaining the first three natural frequencies for different set of pretwist angle (β_0). In Table 1, the results for different number of grid points at Mach number equal to 4 with zero setting angle are presented. Converged results up to four significant digits

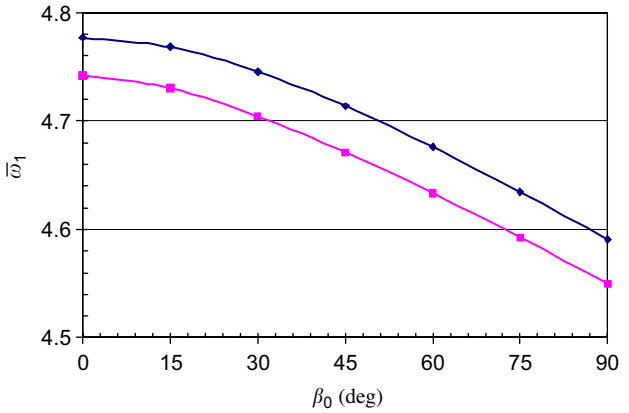

Fig. 6. Variation of natural frequencies vs. pretwist angle ($M_\infty = 4$, $\bar{\Omega} = 3$, $\gamma = 0$, $k = 50$): —◆— Galerkin [11]; —■— present.

are obtained using thirty grid points ($N = 13$). One notes that seven grid points ($N = 7$) is sufficient to obtain results with acceptable accuracy.

Figs. 2–8 are constructed to show the effects of four main system parameters: pretwisting angle (β_0), the Mach number (M_∞), rotating speed (Ω) and material characteristic (k) on the variation of natural frequencies. Wherever possible the obtained results are compared to those of the Galerkin method [11], which are obtained using sixth-order polynomials.

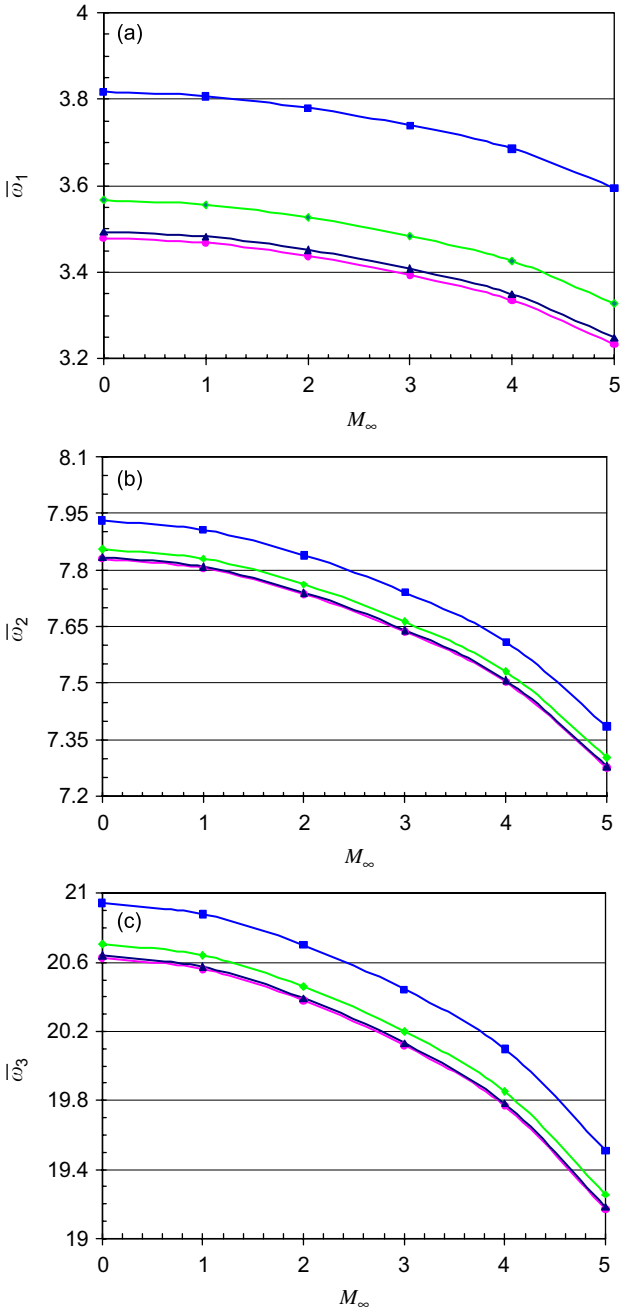

Fig. 7. (a–c) Variation of natural frequencies vs. Mach number for different values of dimensionless rotating speed ($\beta_0 = 45^\circ$, $\gamma = 0$, $k = 0$): $\bar{\Omega} = 0$; $\bar{\Omega} = 0.2$; $\bar{\Omega} = 0.5$; $\bar{\Omega} = 1.0$.

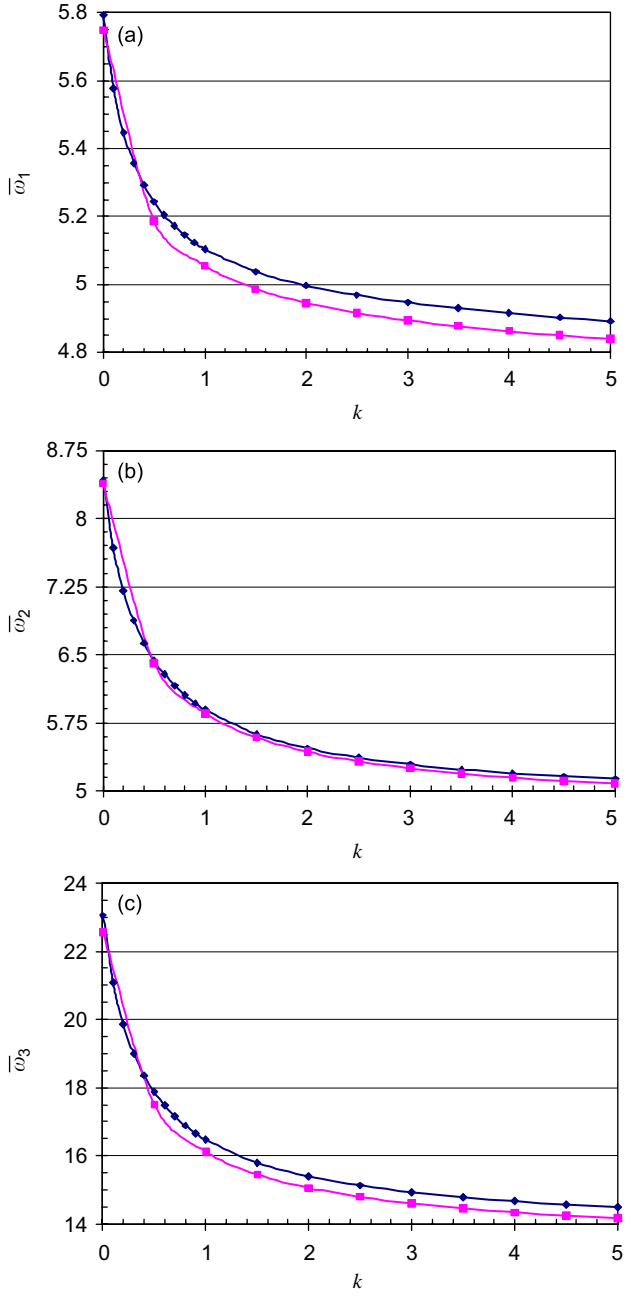

Fig. 8. (a–c) Variation of natural frequencies vs. volume fraction parameter ($M_\infty = 4$, $\beta_0 = 45^\circ$, $\gamma = 0$, $k = 0$, $\bar{\Omega} = 3$): —◆— Galerkin [11]; —■— present.

In Figs. 2(a)–(c), variations of the first three dimensionless natural frequencies against the dimensionless rotating speed for full ceramic constitution at zero Mach number are shown. It is obvious that the DQM results are in close agreement with those of the Galerkin method obtained by Librescu et al. [5].

In Figs. 3(a)–(b), the DQ results for the first two dimensionless natural frequencies are compared with those of the Galerkin method for full ceramic constitution at nonzero Mach number ($M_\infty = 4$). In Figs. 4(a)–(b), the previous characteristics are considered for full metal constitution. In all cases, the relative error between the two methods is less than 1%.

Table 2
Comparisons of CPU time required for calculation of the first three natural frequencies using the DQ and the Galerkin methods ($\beta_o = 15^\circ$, $\gamma = 0$, $k = 0$, $M_\infty = 4$)

DQ Method			Galerkin Method		
Number of grid points (N)	$\bar{\omega}_i$	CPU time (s)[a]	Polynomial order[b]	$\bar{\omega}_i$	CPU time (s)
5	5.89912	0.417	1	6.58380	6.610
	8.53321			10.68061	
	20.80278			–	
7	5.76757	0.426	2	5.87017	18.142
	8.55403			8.66783	
	21.96762			32.32992	
9	5.75797	0.446	4	5.81798	76.984
	8.55147			8.58289	
	22.06454			22.90850	
11	5.75755	0.448	6	5.80719	207.510
	8.55134			8.57695	
	22.06172			22.63645	
13	5.75754	0.459	8	5.80675	463.101
	8.55134			8.57661	
	22.06181			22.63043	

[a]Computer: Intel-Celeron-CPU (1.7 GHz).
[b]Order of polynomial used for displacement components u_0 and v_0.

In Figs. 5 and 6, the influence of pretwist angle for the full ceramic constitution and full metal constitution on the fundamental dimensionless natural frequency with a nonzero Mach number ($M_\infty = 4$) is investigated, respectively. Again good agreements between the DQ and the Galerkin method results are observed.

In Figs. 7(a)–(c), the influences of the rotating speed on the first three dimensionless natural frequencies for fully ceramic constitution are presented.

The effects of the variation of the volume fraction parameter k on the first three dimensionless natural frequencies obtained by DQ and the Galerkin method are shown in Figs. 8(a)–(c).

Comparisons of CPU time required for both the DQ and the Galerkin methods are presented in Table 2. One can see that with much less CPU time, the DQ method yields the converged results. It is interesting to note that the fundamental frequency obtained via the DQM is slightly less than that of the Galerkin method, which predicts the upper bond of the fundamental frequency.

6. Conclusion

The applicability of DQM for vibration analysis of aerothermoelastic thin-walled blades made of FGMs was investigated. The governing equations include the different complexity effects due to the rotation of the blade and the high temperature supersonic gas flow loading. The transverse shear deformation and rotary inertia were considered. The effects of different geometrical parameters and material properties on the convergence and accuracy of the method were investigated using different number of grid points. The results were compared with those of the Galerkin method. Accurate results were obtained using only few grid points, which showed the low computational expense of the method. It is concluded that DQM can be used as an efficient numerical tool for aerothermoelastic problems of structures made of functionally graded materials. Also, the damping matrix appeared in the equation of motions showed that the DQM can be used for damped vibration analysis of FGMs structures.

Appendix A. Review of differential quadrature method

The method of differential quadrature is based on the idea that the partial derivatives of a field variable at the ith discrete point in the computational domain is approximated by a weighted linear sum of the values of the field variable along the line passing through that point which is parallel with the coordinate direction of the derivative [12]. For a one-dimensional field variable $u(x)$, the mth-order derivative with respect to x can be approximated as

$$\left.\frac{\mathrm{d}^m u}{\mathrm{d}x^m}\right|_{(x_i,y_i)} = \sum_{k=1}^{N_x} \bar{A}_{ik}^{(m)} u(x_k) = \sum_{k=1}^{N_x} \bar{A}_{ik}^{(m)} u_k. \tag{A.1}$$

The accuracy of the differential quadrature method is depending on two factors: the first one is the accuracy of weighting coefficients while the second one is the sampling point selection. There are several ways to obtain the weighting coefficients, such as solving Vandermonde system of equations, etc. However, a more accurate method is developed by Shu and Richards [22]. These useful formulas are taken from Shu and Richards [22] by assuming ξ as the dimensionless coordinate variable as

$$\begin{aligned} \bar{A}_{ij}^{(1)} &= \frac{M(\xi_i)}{(\xi_i - \xi_j)M(\xi_j)} \quad \text{for } i \neq j, \\ \bar{A}_{ij}^{(1)} &= -\sum_{j=1, j\neq i}^{N_\xi} \bar{A}_{ij}^{(1)} \quad \text{for } i = j, \end{aligned} \tag{A.2}$$

where

$$M(\xi) = \prod_{j=1, i\neq j}^{N_\xi} (\xi_i - \xi_j).$$

For the second and higher derivatives the weighting coefficients can be evaluated, using the following recurrence relation as

$$\bar{A}_{ij}^{(r)} = r\left[\bar{A}_{ij}^{(r-1)}\bar{A}_{ij}^{(1)} - \frac{\bar{A}_{ij}^{(r-1)}}{(\xi_i - \xi_j)}\right] \quad \text{for } i,j = 1,2,\ldots,N_\xi, \quad i \neq j \text{ and } 2 \leqslant r \leqslant N_\xi - 1 \tag{A.3}$$

and

$$\bar{A}_{ii}^{(r)} = -\sum_{j=1, i\neq j}^{N_\xi} \bar{A}_{ij}^{(r)} \quad \text{for } i = 1,2,\ldots,N_\xi \text{ and } 1 \leqslant r \leqslant N_\xi - 1. \tag{A.4}$$

The simplest way for determining the sampling points is to choose the equally spaced grid points in coordinate direction. But more accurate results can be achieved by using unequally spaced division [12]. It can be as follows:

$$\xi_i = \frac{1}{2}\left\{1 - \cos\left[\frac{(i-1)\pi}{(N_\xi - 1)}\right]\right\}, \quad i = 1,2,...,N_\xi. \tag{A.5}$$

References

[1] L.W. Griffin, D.J. Dorney, Simulations of the unsteady flow through the fastrac supersonic turbine, *Journal of Turbomachinery* 122 (2000) 225–233.

[2] N. Papila, W. Shyy, L.W. Griffin, F. Huber, K. Tran, Preliminary design optimization for a supersonic turbine for rocket propulsion, *Proceedings of the 36th AIAA/ASME/SAE//ASEE Joint Propulsion Conference*, AIAA-2000-3242, 2000, pp. 1–19.

[3] S.Y. Oh, L. Librescu, Thermoelastic modeling and vibration of functionally graded thin-walled rotating blades, *AIAA Journal* 41 (2003) 2051–2060.

[4] L. Librescu, S.Y. Oh, O. Song, Spinning thin-walled beams made of functionally graded materials: modeling, vibration and instability, *European Journal of Mechanics A/Solids* 23 (2004) 499–515.

[5] L. Librescu, S.Y. Oh, O. Song, Thin-walled beams made of functionally graded materials and operating in a high temperature environment: vibration and instability, *Journal of Thermal Stresses* 28 (2005) 694–712.
[6] L. Librescu, *Elastostatics and Kinetics of Anisotropic and Heterogeneous Shell-Type Structures*, Noordhoff International Publishing, Leyden, Netherlands, 1975.
[7] B.V. Sanker, T.J. Tzeng, Thermal stresses in functionally graded beams, *AIAA Journal* 40 (2002) 1228–1232.
[8] J. Aboudi, M. Pindera, S.M. Arnold, Thermoelastic theory for response of materials functionally graded in two directions, *International Journal of Solids and Structures* 33 (1996) 931–966.
[9] J. Aboudi, M. Pindera, S.M. Arnold, Higher-order theory for functionally graded materials, *Composites Part B: Engineering* 30 (1999) 777–832.
[10] A. Berezosvski, J. Engelbrecht, G.A. Maugin, Numerical simulation of two-dimensional wave propagation in functionally graded materials, *European Journal of Mechanics A/Solids* 22 (2003) 257–265.
[11] S.A. Fazelzadeh, M. Hosseini, Aerothermoelastic behavior of supersonic rotating thin-walled beams made of functionally graded materials, *Proceedings of the ASME Sixth International Symposium FSI, Aeroelasticity, FIV and Noise*, ASME-PVP-ICPVT11-93624, 2006, pp. 1–12.
[12] C.W. Bert, S.K. Jang, A.G. Striz, Two new approximate methods for analyzing free vibration of structural components, *AIAA Journal* 26 (1988) 612–618.
[13] C.W. Bert, M. Malik, Differential quadrature method in computational mechanics: a review, *Applied Mechanics Review* 49 (1996) 1–27.
[14] P. Malekzadeh, G. Karami, Vibration of non-uniform thick plates on elastic foundation by differential quadrature method, *Engineering Structures* 26 (2004) 1473–1482.
[15] G. Karami, P. Malekzadeh, A new differential quadrature methodology for beam analysis and the associated DQEM, *Computer Methods in Applied Mechanics and Engineering* 191 (2002) 3509–3526.
[16] P. Malekzadeh, G. Karami, In plane free vibration analysis of circular arches with varying cross section, *Journal of Sound and Vibration* 274 (2004) 777–799.
[17] P. Malekzadeh, M. Farid, A DQ large deformation analysis of composite plates on nonlinear elastic foundations, *Composite Structures* 79 (2007) 251–260.
[18] G. Karami, P. Malekzadeh, S.R. Mohebpour, DQM free vibration analysis of moderately thick symmetric laminated plates with elastically restrained edges, *Composite Structures* 74 (2006) 115–125.
[19] J.N. Reddy, C.D. Chin, Thermomechanical analysis of functionally graded cylinders and plates, *Journal of Thermal Stresses* 21 (1998) 593–626.
[20] G.N. Parveen, J.N. Reddy, Nonlinear transient thermoelastic analysis of functionally graded ceramic metal plates, *International Journal of Solids and Structures* 35 (1998) 4457–4476.
[21] S.H. Pourtakdoust, S.A. Fazelzadeh, Nonlinear aerothermoelastic behavior of skin panel with wall shear stress effect, *Journal of Thermal Stresses* 28 (2005) 147–169.
[22] C. Shu, B.E. Richards, Application of generalized differential quadrature to solve two-dimensional incompressible Navier Stokes equations, *International Journal of Numerical Method in Fluids* 15 (1992) 791–798.